Classical and Quantum Gravity

PAPER

Improving sensitivity and duty-cycle of a double torsion pendulum

To cite this article: M Bassan *et al* 2019 *Class. Quantum Grav.* **36** 125004

IOP Publishing Classical and Quantum Gravity

Class. Quantum Grav. 36 (2019) 125004 (16pp) https://doi.org/10.1088/1361-6382/ab206b

Improving sensitivity and duty-cycle of a double torsion pendulum

M Bassan[1,2], M De Laurentis[3,4], R De Rosa[3,4,9], L Di Fiore[4], L Errico[3,4], F Garufi[3,4], A Grado[4,5], Y Minenkov[2], G Pucacco[1,2], V Spagnuolo[3,4], R Stanga[6,7] and M Visco[2,8]

[1] Dipartimento di Fisica, Università di Roma 'Tor Vergata', I-00133 Roma, Italy
[2] INFN—Sezione Roma Tor Vergata, I-00133 Roma, Italy
[3] Dipartimento di Fisica, Università di Napoli 'Federico II', I-80126 Napoli, Italy
[4] INFN—Sezione di Napoli, I-80126 Napoli, Italy
[5] INAF—Osservatorio Astronomico di Capodimonte, I-80131 Napoli, Italy
[6] Dipartimento di Fisica ed Astronomia, Università degli Studi di Firenze, I-50019 Firenze, Italy
[7] INFN—Sezione di Firenze, I-50019 Firenze, Italy
[8] INAF—Istituto di Astrofisica e Planetologia Spaziali, I-00133 Roma, Italy

E-mail: rosario.derosa@na.infn.it

Received 7 February 2019, revised 24 April 2019
Accepted for publication 9 May 2019
Published 28 May 2019

Abstract

In this paper the enhancement of the sensitivity and of the duty-cycle of a double stage suspended torsion pendulum are described. The increase in sensitivity, both for force and torque measurements, was obtained rearranging the pendulum mechanics, reducing the value of the suspended masses and moments of inertia and by adopting additional read-outs based on optical levers. The improvement of the duty-cycle was obtained by controlling the suspension point of the pendulum to reduce the effect of seismic noise on the translation resonances of the system. The reduction of these motions allowed continuous operation for three weeks, in high sensitivity regime of the read-out electronics, resulting in a force sensitivity of $6 \cdot 10^{-11}$ N $(\sqrt{\mathrm{Hz}})^{-1}$ and a torque sensitivity of 10^{-14} Nm $(\sqrt{\mathrm{Hz}})^{-1}$ around 10 mHz.

Keywords: torsion pendulum, small force measurement, noise reduction

(Some figures may appear in colour only in the online journal)

[9] Author to whom any correspondence should be addressed.

1. Introduction

Torsion pendulums are excellent instruments for the measurement of small forces and torques. Historically they have been used by Coulomb to study the electrostatic force [1] and by Cavendish to measure the gravitational constant [2]. Presently they are still widely used in many experiments that investigate the effect of very small actions.

A not complete list of frontier applications of torsion pendulum includes: accurate measurements of the gravitational constant [3, 4], study of deviations from inverse square law in gravitation [5], Casimir force measurements [6], test of equivalence principle [7].

Besides these specific applications in fundamental physics, torsion pendulums are very effective in all measurements requiring almost free-fall conditions; in particular a class of such equipments was developed [8–10] and used in the past years for the characterization of the gravitational reference sensor (GRS) [11] used in the LISA pathfinder (LPF) mission [12], launched in December 2015. The success of LPF [13–15] was also due to the careful and detailed characterization work performed with torsion pendulums [16].

The double torsion pendulum named PETER (from Italian PEndolo Traslazionale E Rotazionale, namely rotational and translational pendulum) [10], was specifically developed to characterize the sensing and actuation crosstalk of the GRS. This was possible since, among all the 6 degrees of freedom (DOF) of the suspended test mass (TM), two of them, corresponding to the rotation of the upper and lower suspension fibers, are characterized by a very low stiffness. This is a unique feature of PETER.

After the end of LPF mission, the double pendulum was upgraded to enhance its sensitivity and duty cycle.

The motivation for the upgrade mainly came from the high residual force noise of the original set-up. In fact, the past measurement campaigns, aimed to the characterization of the actuation crosstalk, gave satisfactory results for torques contaminations induced by force actuations [17], and only provided upper limits in the reversed actuation scheme [18]. Even with this limitation these results confirmed that the actuation crosstalks were well inside the requirements for LPF: the measured crosstalk was indeed less than 0.2% in the most relevant region of the GRS, i.e. within $\pm 10\ \mu$m from its center [19]. Nevertheless, the high residual force noise made impossible their complete characterization within the pendulum dynamics.

During the same measurement campaign it also emerged that the duty-cycle of the pendulum was strongly affected by the local microseismic noise, depending, in turn, by the weather conditions. Occasionally, in case of bad weather, this prevented us in performing long enough measurements in standard conditions, due to the saturation of the sensing system of the GRS: indeed the pendulum oscillated with such a large amplitude that we were forced to operate the GRS in the so-called wide measurement range, finally resulting in a lower sensitivity of the apparatus.

The upgrade of the pendulum resulted, at the end, in a reduction of residual force noise by a factor 5 and a factor 2 in residual torque noise with respect to the previous performances. Moreover, the improvement of the duty-cycle allowed continuous measurements, with GRS operating at high sensitivity, for periods lasting longer than three weeks.

These improvements will be eventually useful for a future characterization of the LISA GRS, even if the requirements in terms of crosstalks are not yet defined. Indeed, the details of the LISA mission are still under discussion. Anyway, the reduction in force noise will allow to measure the crosstalk with at least five times better accuracy.

Moreover, the improvements will allow the use of PETER, with some further modification, also for other fundamental gravity measurements, like test of inverse square low, or G measurements. Indeed for such measurements both high duty-cycle and low residual noises are required. Moreover, the possibility to estimate, at the same time, the force and the torque acting on the TM, represents a useful tool for investigations on systematic errors [20].

The paper is organized as follow: in section 2 the main elements of the apparatus, before and after the upgrade are described, in section 3 the performances of the upgraded system, due to the mechanics rearrangement and optical read-out (ORO) are compared with the old ones, in section 4 the implementation of the suspension point control is described, finally, in section 5, the performance of the full upgraded pendulum, in terms of sensitivity and duty cycle, are reported.

2. The PETER apparatus and its characteristics

The main characteristic of PETER is the possibility to measure simultaneously both the force and the torque acting on the TM. This is due to its particular structure: a first fiber holds a cross-bar and a second fiber, holding the TM, is fixed at one extreme of the cross-bar. Three other masses (load TMs), in symmetrical positions below the other extremes of the cross-bar, act as counterweights. In this way a force acting on the TM, being a torque on the cross-bar, produces a rotation of the upper fiber, while a torque acting on the TM, mainly produces a rotation of the lower fiber. Of course this is true if the frequency of the actuations is higher than the torsional resonances and lower than the translation resonances. By measuring translation and rotation of the TM it becomes possible to simultaneously estimate the force and the torque acting on the TM [21, 22].

Before the upgrade, the counterweights were rigidly fixed to the cross-bar through three long rigid legs. An additional leg was also placed around to lower fiber to balance the mass, and the vertical distribution, of the other legs. Moreover all the information about the pendulum motion were derived only by the motion of the TM, using the signals coming from the capacitive read-out of the GRS [11].

The pendulum can be described as a cascade of two rigid bodies, strongly simplifying its dynamics, as extensively described in [22]. On the other hand, this configuration has three main drawbacks: (1) the legs increase both the mass and the moment of inertia of the cross-bar, resulting in a sensitivity reduction in the detected force, since the same force intensity produces a smaller displacement of the mass; (2) the center of mass of the upper stage of the pendulum is not located along the upper suspension wire but mainly along the y axis (see figure 1), resulting in a direct coupling between the suspension point motion (mainly due to seismic noise) [23] and the cross-bar; (3) since the only probe of the pendulum is the GRS at the TM level, the detected displacement of the TM along x axis is due not only to the cross-bar rotation around z but also to the pendulum motion around y, as explained by (4) of [22].

Another strictly technical problem, arising from the presence of rigid legs, was the balancing of the cross-bar. Indeed, assembling tolerances cause the rigid legs to slightly deviate from vertical, thus producing a further lateral displacement of the center of mass of the first stage, that has to be balanced with suitable counterweights placed on the upper surface of the cross-bar further increasing both its weight and moment of inertia.

With the aim to remove all the known drawbacks, the rigid legs were eliminated and all the load masses were suspended to the cross-bar with suitable fibers. As a further improvement two additional sensors were added on the system, both based on optical levers. The first one was added at the level of the cross-bar to measure directly its rotation. The second one was added at level of the TM to measure, with higher sensitivity, the rotation and the translation of the TM.

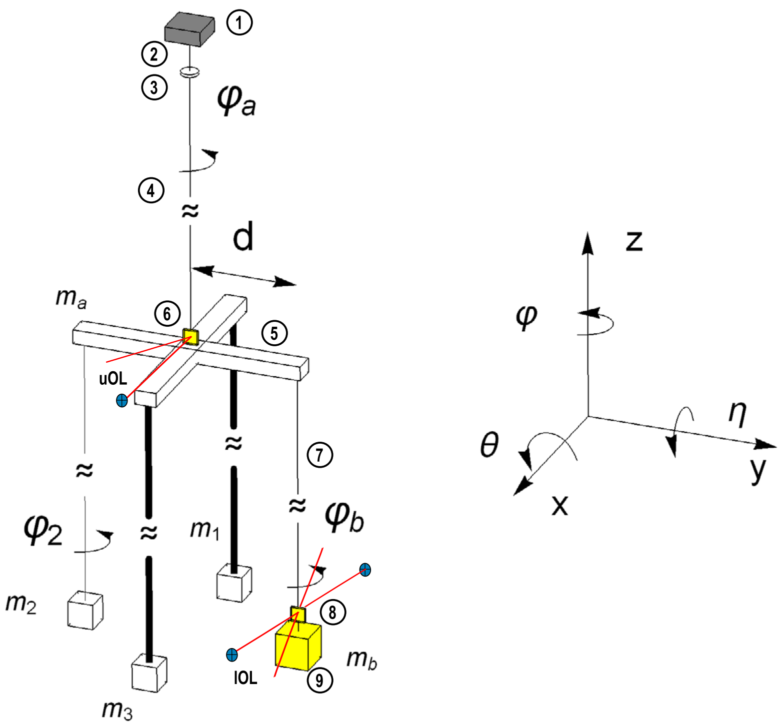

Figure 1. A sketch of the PETER pendulum. From top to bottom it is possible to distinguish: the PZT translator (1), the pre-hanger (2), the magnetic damper (3), the upper fiber (4), the cross-bar (5) equipped with the mirror (6) used for the upper optical read-out (uOL), the lower fiber (7) with the mirror (8) for the lower optical read-out (lOL) and the TM (9). The reference system used to describe the pendulum is also shown; the origin is the suspension point of the upper fiber.

In order to simplify the dynamics of the systems, even with all the suspended TMs, only the load mass placed at the opposite side of the cross-bar, with respect to the main TM, was hung by thin fiber (hereafter TM_2). The two remaining load TMs were suspended with thicker fibers (100 μm radius) to have their torsional resonances above 0.1 Hz, producing no perturbation in the measurement band spanning from few mHz to about 0.1 Hz.

The additional read-out of the cross-bar was implemented by an optical lever: a beam from a fiber coupled super luminescent diode impinge on a mirror placed on the center of the cross-bar, and the motion of the reflected beam is measured by a quadrant photodiode. It is very easy to add this simple read-out system: it requires few modifications of the apparatus and the results are very effective [24].

The second additional read-out on the TM, was implemented by a pair of optical levers, similar to the one described above. The two beams impinges on the opposite faces of the mirror fixed on the top of the TM, and by a suitable linear combination of the signals provided by two quadrant photodiodes, it is possible to extract the translation and the rotation of the TM.

As an additional upgrade, the apparatus was equipped with a three axial piezoelectric (PZT) translation stage, used as top stage of the whole pendulum. This make it possible to move the main suspension point of the pendulum along the three axis.

The upgraded pendulum is schematically shown in figure 1. From top to bottom it is possible to distinguish the PZT translation stage at the suspension point, the pre-hanger: a short fiber ending with an aluminum disk inserted between two magnetic rings (not shown in the figure) used for the magnetic damping of the main pendular motions, the upper fiber, the mirror used for the upper optical lever at the cross-bar level, the cross-bar with all the lower fibers suspending the TM and the other load mass, and the mirror for the lower ORO placed just on the top of the TM. The reference system used in the paper is also shown in the figure. Its origin is placed on the suspension point of the upper fiber. The rotations around the vertical axis are indicated by φ. In particular: φ_a is the rotation of the cross-bar, while φ_b and φ_2 are the rotations of TM and TM_2, respectively, with respect to the cross-bar.

By using a simplified model, taking into account only the torsional motions around z, and assuming small rotations, the system can be described by the following equations:

$$\begin{aligned} &I_c\ddot{\varphi}_a + \gamma\dot{\varphi}_a - \gamma_b\dot{\varphi} - \gamma_2\dot{\varphi}_d + k\varphi_a - k_b\varphi - k_2\varphi_d = \tau_a + d(F_b - F_2) \\ &I_b\ddot{\varphi} + \gamma_b\dot{\varphi} - \gamma_b\dot{\varphi}_a + k_b\varphi - k_b\varphi_a = \tau_b \\ &I_2\ddot{\varphi}_d + \gamma_2\dot{\varphi}_d - \gamma_2\dot{\varphi}_a + k_2\varphi_d - k_2\varphi_a = \tau_2 \end{aligned} \quad (1)$$

where

$$\begin{aligned} &I_c = I_a + (m_b + m_1 + m_2 + m_3)d^2 \\ &\gamma = \gamma_a + \gamma_b + \gamma_2; \quad k = k_a + k_b + k_2 \\ &\varphi = \varphi_a + \varphi_b; \quad \varphi_d = \varphi_a + \varphi_2 \end{aligned}$$

being: I_j, γ_j and k_j the moment of inertia, dissipation factor and elastic constant of the j-pendulum ($j = a, b, 2$), F_b and F_2 the forces, along the x direction, acting on the TM and TM_2, τ_a, τ_b and τ_2 the vertical component of the torques acting on the cross-bar, the TM and the TM_2 respectively, I_c the full moment of inertia of the cross-bar, as it is modified by the presence of the suspended TMs with masses m_j ($j = b, 1, 2, 3$), φ the full rotation of the TM with respect to suspension point and φ_d that of the TM_2, d the length of the cross-bar arms.

The full rotation of the TM and its translation along the x axis, $\varphi(t)$ and $x(t)$, are directly sensed by the GRS and by the lOL, while the optical lever on the cross-bar senses its rotation: $\varphi_a(t)$. No additional sensor was added to measure the rotation and translation of TM_2. At first approximation $x(t) \approx \mathrm{d}\varphi_a(t)$, but even at low frequency the full translation of the TM is perturbed by the pendular motion of the system along the other DOF [22], resulting in an overestimation of the cross-bar rotation if extracted by using only the TM translation.

The force and the torque acting on the TM, F_b and τ_b, can be estimated by solving the system (1). Since the motion of TM_2 is not monitored, the solution is only approximated, but it is valid above the torsional resonances of the pendulum and, of course, below the translational resonances that are not described by this simplified dynamics. This is equivalent to set $F_2 = 0$ in (1). Moreover the torque acting directly on the upper stage will be neglected, resulting in some overestimation of the force F_b. This assumption is well justified by the force and torque measurements described in [17].

The main parameters of PETER, before and after the upgrade, are summarized in table 1. Beside the masses and the moment of inertia of the suspended elements, in the table are also listed: the length (l_a, l_b) of the upper and lower fibers, their radius (r_a, r_b, r_2), the measured elastic constant of the fiber (k_a, k_b), the torsional resonance frequencies of the system (f_a, f_b, f_2) and their quality factor (Q_a, Q_b, Q_2).

The mass of the cross-bar and TMs, the length and the radius of the suspension wires were measured before the system assembly. The elastic constants of the fibers were estimated by measuring the period of a simpler torsion pendulum, especially designed, composed by very

Table 1. Main parameter of the pendulum before and after the upgrade.

Parameter	Before upgrade	After upgrade	Uncertainty	Unit
d	0.150	0.150	0.001	m
l_a	0.701	0.706	0.001	m
l_b	0.789	0.781	0.001	m
m_a	1.307 74	0.419 32	$4 \cdot 10^{-5}$	kg
m_b	0.093 84	0.097 90	$4 \cdot 10^{-5}$	kg
m_2	—	0.097 82	$4 \cdot 10^{-5}$	kg
I_c	$2.90 \cdot 10^{-2}$	$1.14 \cdot 10^{-2}$	10^{-4}	kg m^2
I_b	$4.29 \cdot 10^{-5}$	$4.28 \cdot 10^{-5}$	10^{-7}	kg m^2
I_2	—	$4.05 \cdot 10^{-5}$	10^{-7}	kg m^2
k_a	$1.94 \cdot 10^{-6}$	$8.36 \cdot 10^{-7}$	$8 \cdot 10^{-9}$	kg m^2 s^{-2}
k_b	$6.9 \cdot 10^{-9}$	$7.3 \cdot 10^{-9}$	$3 \cdot 10^{-10}$	kg m^2 s^{-2}
r_a	50	40	4	μm
r_b	12.5	12.5	1	μm
f_a	1.307	1.370	0.002	mHz
f_b	2.052	2.079	0.002	mHz
f_2	—	2.093	0.002	mHz
Q_a	640	640	20	—
Q_b	470	470	20	—
Q_2	—	500	20	—

symmetric masses, with known moment of inertia. The resonance frequency were estimated by the spectra of the signal $\varphi(t)$ and $x(t)$, while the quality factors were estimated by ring-down measurements of the resonances themselves. The moment of inertia were computed by combining the resonance frequencies and the elastic constants following (1).

3. Performances after the system upgrade

The sensitivity of the system, in terms of force and torque acting on the TM, can be estimated, on the basis of the previous assumptions, by measuring the motion of the TM using the GRS signals, in particular $x(t)$ and $\varphi(t)$. After the upgrade, thanks to the new ORO systems, it is also possible to estimate force and torque by using $\varphi_a(t)$, $\varphi(t)$ as measured by these sensors.

Figure 2 summarizes the result of the upgrade. In particular, the left panel shows a comparison between the amplitude spectral densities (ASD) of the rotation $\varphi_a(t)$ as measured by the GRS ($\varphi_{a,\mathrm{GRS}}$, black curve), before the upgrade, and the same quantity as measured by the upper optical lever ($\varphi_{a,\mathrm{ORO}}$, red curve) after the upgrade. In the right panel there is instead a comparison of the ASD of $\varphi(t)$ measured by the GRS (φ_{GRS}, black curve), before the upgrade, and the same quantity as measured by the lower optical levers (φ_{ORO}, red curve) after the upgrade. The electronic noise of the GRS (black dashed line) and ORO (red dashed line) are also shown, together with the expected thermal noise (blue dashed line).

The noise due to the radiation pressure of the optical levers results negligible. In fact the power impinging on the TM is about 0.1 mW, and the resulting DC force, on the TM, is about $3 \cdot 10^{-13}$ N. This value is already lower than the minimum detectable force and it is even lower at higher frequencies.

Thermal noise was estimated by using the model described by (1), assuming a viscous damping.

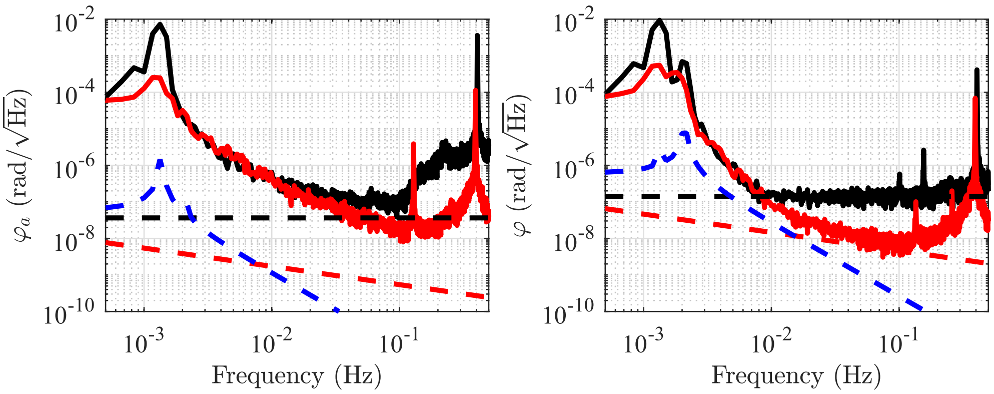

Figure 2. Amplitude spectral density of the two rotational DOF of the pendulum: upper stage (left panel) and lower state rotation (right panel), before (black) and after the upgrade (red). The dashed curves are the GRS sensing noise (black), the ORO sensing noise (red) and the expected thermal noise (blue).

The additional measurement of the TM translation, measured by the lower optical lever is not reported since it results equivalent to $\varphi_{a,\mathrm{GRS}}$: their spectra are practically overlapped.

The spectrum of φ_{GRS} is limited by the read-out electronic noise in the band 10–200 mHz. The spectrum of $\varphi_{a,\mathrm{GRS}}$ is far from that limit and it is dominated, in the same band, by the displacement noise coupling with the η_a and η_b DOFs [22]. This is more evident from the comparison with the spectrum of the same signal sensed by the upper optical lever ($\varphi_{a,\mathrm{ORO}}$), that does not suffer the same coupling.

At low frequencies both φ_a and φ are dominated by the residual torsional motions, while for higher frequencies the limit is given by the coupling with seismic noise, especially at the translational resonance frequency that strongly enhance this kind of disturbance (≈0.4 Hz).

The residual force and torque acting on the TM, as estimated by the measurements reported in figure 2, are shown in figure 3. In the figure the black curves represent the performances before the upgrade, while the red curves are the present limit. The improvements due both to the rearrangement of the mechanics and to the use of ORO are quite evident.

The residual torque noise, at least in the band 4–20 mHz, approaches the thermal noise, while the force noise is still far from the thermal limit. This is due to the higher rejection of torsional motion to the seismic noise, while for the translational motions, that are still involved in the force measurement, even with the ORO on the upper stage, the coupling is much higher.

4. Suspension point control

Two main limits were recognized for the sensitivity and duty-cycle of the pendulum. The first one is due to a slow drift of TM and cross-bar in their torsional motions, mainly due to the fibers unwinding and slow changes of environmental conditions (i.e. temperature). The second one is due to the translational resonance of the pendulum, since it is inside the 0.1–1 Hz band, that is strongly affected by the microseism due to the sea waves [25]. This seismic background noise, that is always present and enhances in bad weather condition, produces a strong pendular motion especially along x and y directions, that can exceed the sensor range, both for GRS and optical levers. In this case it is still possible to measure the pendulum motion by increasing the range of the sensors, but this imply a reduction of their sensitivity and consequently a degradation of the whole system performances.

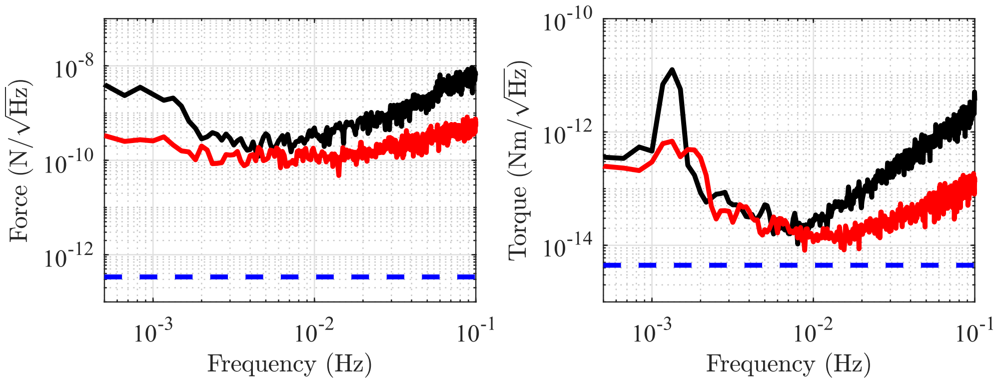

Figure 3. Residual force (left panel) torque (right panel), before (black) and after (red) the upgrade. The dashed blue line is the expected thermal noise.

The first limit can be easily overcome by using the electrostatic actuation available on the GRS [11, 26] performing all the measurements in closed loop condition, keeping the TM in the center of the GRS and reducing the amplitude of the torsional oscillations. In this case it is important to limit the action of the feedback at very low frequencies to avoid introducing any control noise in the relevant measurement band. To this aim the unity gain of the loops was set to 3 mHz and a steep roll-off was applied above this frequency.

The second limit cannot be overcome as the first one, since the actuations performed by the GRS are not effective for translational DOFs, due to the very limited force they can apply on the TM. In particular, the maximum force exerted by the electrostatic actuators of the GRS is about $5 \cdot 10^{-8}$ N, while the force required to move the TM by only 10 μm along x is of the order of 10^{-5} N. Since the amplitude of the translation motion induced by the microseism can even exceed 250 μm, it is clear that no feedback is possible with such actuator.

In this case the solution is to actively reduce the motion of the pendulum suspension point. A seismometer can be used to measure the ground motion in the band 0.1–1 Hz and the suspension point can be moved, by using the PZT translation stage placed on the top of the pendulum, to compensate the ground motion.

Two kinds of seismometer are used to measure the ground motion: a force balance accelerometer (FBA-ES-T by Kinematrics) and a velocimeter (LE-3D/5s by Lennartz). Both seismometers are three-axial. The accelerometer measures the ground acceleration up to about 200 Hz, while the velocimeter returns the ground velocity in the band 0.2–50 Hz. The PZT stage is the model P-562.6CD by Physik Instrumente, that is a 6-DOF stage with a range of 200 μm for each translation. The stage uses internal sensors and operates in closed loop condition.

The PZT stage is aligned to the pendulum reference system and the same is done for the seismometers. The alignment of the PZT was verified by moving the stage along each axis and measuring the corresponding motion of the TM. The alignment of the seismometers was verified by measuring the coherence between the seismic noise along the three axis and the respective DOF of the TM. In both cases the residual misalignment was less than 5%.

In this way a ground motion along x can be compensated acting, in the opposite direction, on the x axis of the PZT and the effect is visible on the x DOF of the TM. The same for the y axis. The control of the suspension point is performed in feed-forward, in order to avoid stability issues with a feed-back system.

To select the best seismometer to use for this application both were tested, in different periods, as reference for the ground motion measurement. Since the output of the two instrument is different, and the signal to drive the PZT is proportional to the ground motion, two different filters were applied in the case of the accelerometer and velocimeter.

The first approach was to compensate the ground motion in the band 0.1–1 Hz. Then a more selective compensation was used.

4.1. Full band compensation

The accelerometer was the first to be used as reference sensor, since its response, in the required band, is practically flat. The compensation should not act at low frequencies, since the accelerometer response is dominated by electronic noise for $f < 0.1$ Hz. The compensation filter $C_a(s)$, is composed with two zeros in the origin and two couples of complex conjugate poles, giving a 4th order Butterworth low pass filter, with the cutoff frequency at $f_c = 45$ mHz. The two zeros reduce the action of the compensation at low frequencies, while the four poles, above f_c give the needed double integration of the acceleration signal to build the ground displacement signal. The cutoff frequency was placed well before the compensation band edge (0.1 Hz) to allow the phase of the filter to reach a value close to $-\pi$, that is the ideal value for a double integrator.

The same compensation was applied using the velocimeter as reference sensor, but in this case it was necessary to take into account the instrumental response, that is not flat enough in the compensation band. In particular, the manufacturer provides the following instrument response $R_v(s)$:

$$R_v(s) = \frac{v(s)}{v_0(s)} = \frac{s^3}{(s + 2\pi f_1)(s^2 + \frac{2\pi f_2}{\sqrt{2}} s + 4\pi^2 f_2^2)} \tag{2}$$

where $v(s)$ and $v_0(s)$ are the Laplace transform of the velocimeter output and ground velocity respectively, $f_1 = 0.0462$ Hz and $f_2 = 0.2$ Hz.

By knowing the instrument response it is possible to design a compensation filter that behaves as an integrator in the compensation band, and minimizes its action at low frequencies. In particular the following compensator has been implemented:

$$C_v(s) = K \frac{s(s + 2\pi f_1)(s^2 + \frac{2\pi f_2}{\sqrt{2}} s + 4\pi^2 f_2^2)}{(s + 2\pi f_3)(s^2 + \frac{2\pi f_4}{\sqrt{2}} s + 4\pi^2 f_4^2)(s^2 + \frac{2\pi f_5}{\sqrt{2}} s + 4\pi^2 f_5^2)} \tag{3}$$

where the zeros at f_1 and f_2 take into account the instrument response, the additional poles at $f_3 = f_1/10$ and $f_4 = f_2/10$ are needed to cancel the effect of the previous zeros in the compensation band, the zero in the origin has the effect to reduce the gain at low frequencies, the two poles at $f_5 = 5$ mHz provide for the integrator behavior in the compensation band, finally, the constant K is chosen to have the right gain in the compensation band.

In figure 4 the two compensation filters, both for the accelerometer and the velocimeter, are shown in comparison with the required behavior: a double integrator for $C_a(s)$ and a simple integrator for $C_v(s)$. In the case of the velocimeter it is also shown the effect of the filter on the ground velocity, i.e. removing the instrument response.

The compensation is obtained by applying the signal to the PZT stage, as shown in figure 5.

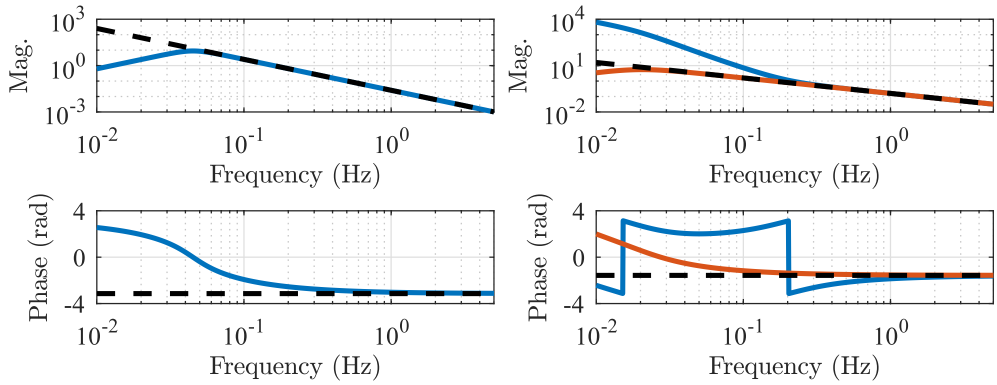

Figure 4. Bode diagram of the filters used for compensation: accelerometer (left panel) velocimeter (right panel). For both the required behavior is shown (dashed line). In the case of velocimeter the filter response with respect to the ground velocity is also reported ($C_v(s)R_v(s)$, red line).

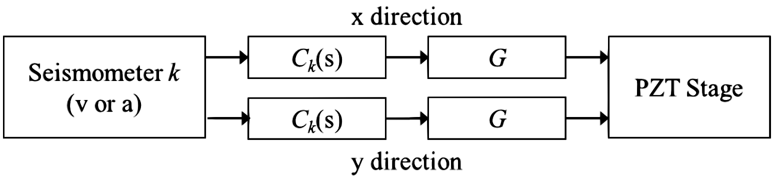

Figure 5. Compensation scheme: the signals from the seismometers are filtered and applied to the corresponding DOF of the PZT stage.

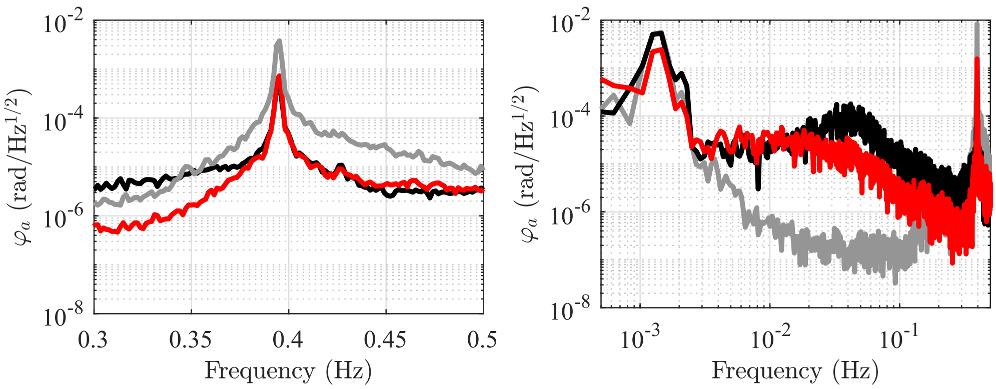

Figure 6. Effect of the compensation. Left panel: reduction of the φ_a motion with active compensation. Right panel: extra noise due to the compensation at low frequencies. Black and red lines: compensation with accelerometer and velocimeter respectively, gray line: no compensation.

The two compensation filters give the expected behavior in reducing the motion of the pendulum in the band 0.1–1 Hz. In particular a reduction of about a factor 4–5 is easily achieved in most environmental conditions. This reduction is observed with both reference seismometers. However, in spite of the designed low gain at low frequencies of both compensation filters, a degradation of the pendulum performances is observed when the compensation is active. Figure 6 summarizes these results. The black and red curve are the spectra of $\varphi_{a,\mathrm{GRS}}$ with active compensation using the accelerometer or the velocimeter as reference sensor, respectively; the gray curve is the spectrum with no compensation. In the left panel the reduction of the motion in the compensation band is well visible with the two different reference seismometers with respect to the uncompensated condition. In the same conditions, as clearly shown in figure 6, right panel, a strong extra noise, fully induced by the out-band effects of the compensation is visible.

Clearly the full band compensation is not the proper solution, since the advantage of the reduction of the translational motions is completely overtaken by the large noise injected at low frequencies.

A different compensation scheme is needed.

4.2. Narrow band compensation

The new compensation scheme was chosen on the basis of the following observation: the larger translational motions of the pendulum, only occur at selected resonance frequencies that are excited by the microseism. These frequencies are very stable in time and were accurately measured by the spectra of $x(t)$ and $y(t)$ computed over several hours of measurement time.

The most relevant resonance corresponds to the normal mode where the two pendulum stages move in phase at: $f_r = 0.3974$ Hz and is degenerate along x and y.

The compensation filter is designed in order to be relevant only at the resonance frequency, moreover, at this frequency it has to act as a simple or a double integrator depending on the reference seismometer.

The first condition was implemented with a filter with $2n$ complex conjugate poles at frequency f_r and m zeros in the origin:

$$C(s) = \frac{s^m}{(s^2 + s\frac{2\pi f_r}{Q} + 4\pi^2 f_r^2)^n}. \tag{4}$$

It is necessary to take into account the response of the seismometers: $R_a(s) = 1$, since the accelerometer response is almost flat, while $R_v(s)$ given by (2). Being p the ground motion along one of the axis and q the corresponding seismometer output, it results:

$$q_v = R_v(s)sp \;\; \text{and} \;\; q_a = R_a(s)s^2p. \tag{5}$$

Since the compensation signal to send to the PZT actuator is $C(s)\,p$, using (5) the compensation filter has the form:

$$C_v(s) = G\frac{C(s)}{sR_v(s)} \tag{6}$$

$$C_a(s) = G\frac{C(s)}{s^2R_a(s)} \tag{7}$$

for the velocimeter and the accelerometer respectively. G is the gain of the filter.

The phase of $C(s)$ has to be zero when $s = 2\pi i f_r$. Since the m zeros in the origin introduce a phase of $m\pi/2$ and the $2n$ poles give a phase of $-n\pi/2$ at f_r, it is necessary that $m = n$. The gain is then fixed by the condition $C(2\pi i f_r) = 1$.

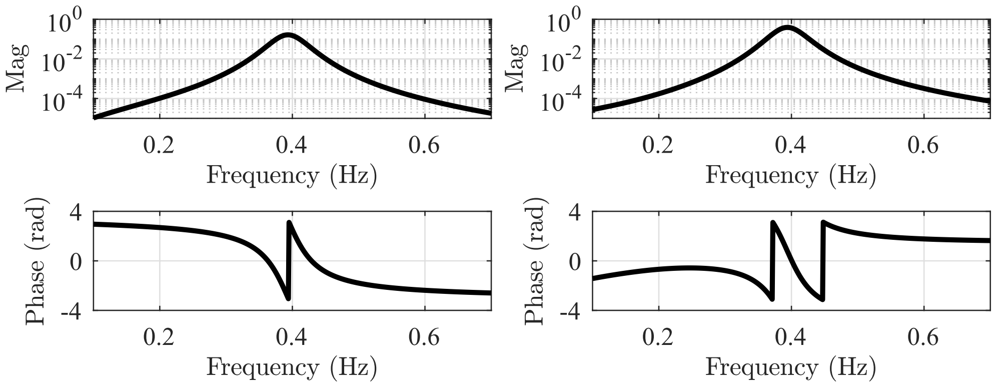

Figure 7. Transfer function of the narrow band compensation filter. Left panel: accelerometer, right panel: velocimeter.

Also in this case the compensation is obtained by applying the signal to the PZT stage as shown in figure 5.

The narrow band compensation filters were implemented by choosing $n = 4$ and $Q = 6$. Figure 7 shows the designed transfer functions, both for the velocimeter and accelerometer. It is evident the very low gain of the filters far from the resonance.

5. Result and discussion

To verify the effectiveness of the narrow band compensation a long duration test was performed on the pendulum. The compensation was first switched on using the accelerometer as reference sensor, then the reference was switched on the velocimeter, finally the compensation was switched off. Each condition was maintained for 6 h and this cycle was repeated for several days.

The results of this test are summarized in figure 8. The upper panel of figure shows the compensation condition: the continuous and dashed lines represent the compensation with the accelerometer and the velocimeter respectively. If a compensation is active the relative value is 1, otherwise it is zero. The lower panel reports the ratio between the pendulum motion along a direction at frequency f_r, measured by the GRS, and the rms of the seismic noise, along the same direction, measured by the accelerometer, in a band centered at f_r with a width of $\Delta f = 60$ mHz. Both the pendulum motion and the seismic noise are estimated by using the ASD of 300 s long time series of the signals. The three lines refer to the x (black), y (red) and z (blue) directions.

The ratio between the motion and rms seismic noise is a good indicator of the compensation efficiency, since it is almost independent by the environmental conditions. An high value of this normalized pendulum motion represents a large motion at the relative resonance, independently from the level of seismic noise acting in the selected period.

The correlation with the compensation condition and normalized motion amplitude, is very clear as shown in the second panel of figure 8. The main effect is along the x and y directions: the motion is reduced by a factor 10 or better.

The reduction of the motion along z, observed when the compensation is active, is due to the coupling of the horizontal and vertical motions introduced by the GRS (geometrical or electronic asymmetries and non-linearities [27]) and not to direct compensation. In fact, whether the compensation along z is active or not, the observed motion reduction does not change.

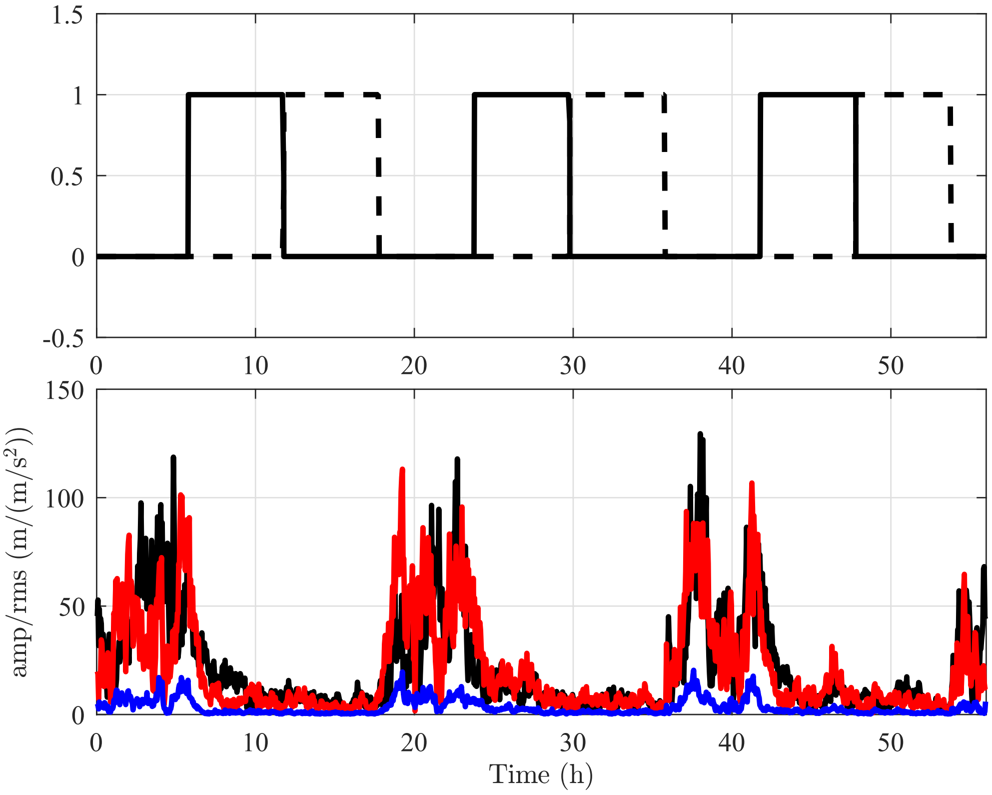

Figure 8. Test of the narrow band compensator. The upper panel shows the compensation condition off: 0, on: 1, full line: accelerometer, dashed line: velocimeter. The lower panel reports the ratio between the motion of the TM at f_r, measured by GRS, and the corresponding accelerometer signal in a small band around the same frequency. The three lines refer to x (black), y (red) and z (blue) directions.

The long test period performed by switching the two reference seismometers was also useful to select the best compensation condition.

Figure 9 shows the motion amplitude at f_r versus seismic noise rms in the small band around the resonance frequency. In the figure each column refers to a direction: x, y and z respectively. The colors represent the compensation condition: gray—no compensation, black and red—compensation with accelerometer or velocimeter as reference sensor respectively. In the second row only the data with active compensation are reported to better identify the effect of the selected seismometer.

The compensation requires some time before becoming effective after its activation, as it is clearly shown in figure 8, due to the high quality factor of the pendular motion. To avoid any kind of bias in evaluating the compensation effectiveness with the two different seismometers, the first two hours of data, after any compensation change, are not included in figure 9.

By comparing the amplitude of motion in the two different compensation conditions, it is evident, by the distribution of the points in the second row of figure 9, that the use of the velocimeter, as reference sensor, allows a more effective motion reduction.

The better performance of the velocimeter, as reference sensor, is mainly due to its higher sensitivity at the relevant frequency: 400 V/m/s instead of 4 V/m/s^2 for the accelerometer, that

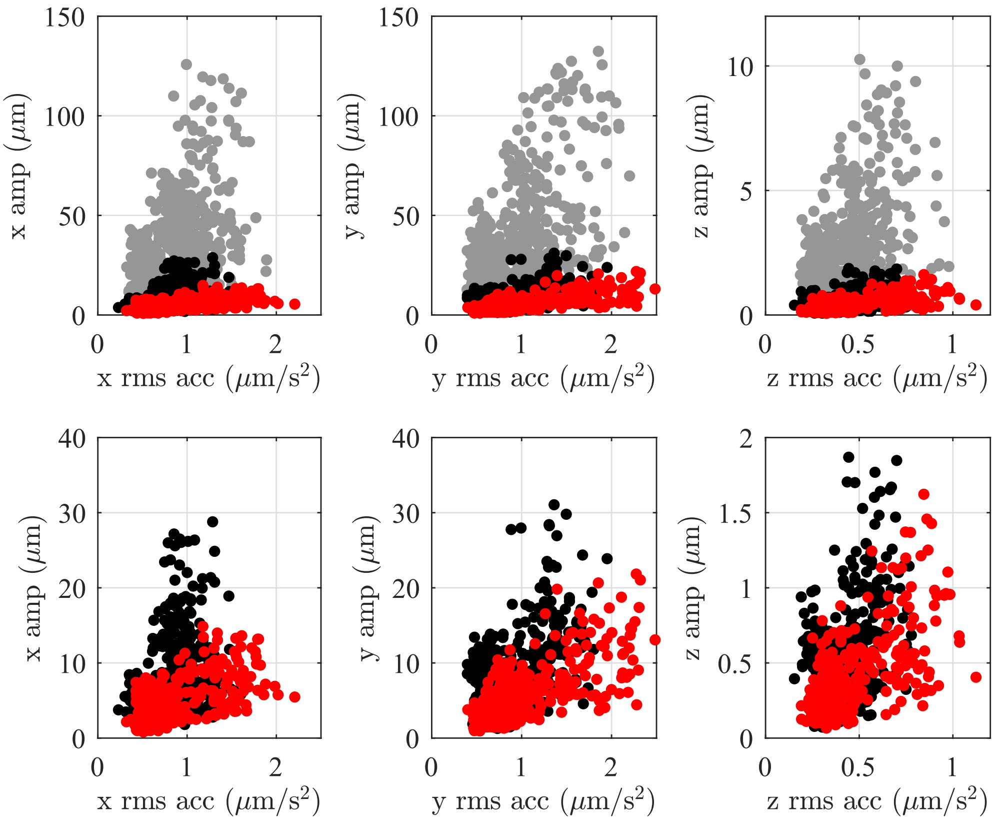

Figure 9. Amplitude of the motion at the resonance frequency versus seismic noise rms. The different colors refer to the compensation conditions: gray—no compensation, black—accelerometer, red—velocimeter. Each column is relative to a direction: x, y and z. The second row shows a zoom of the first one but only with active compensation.

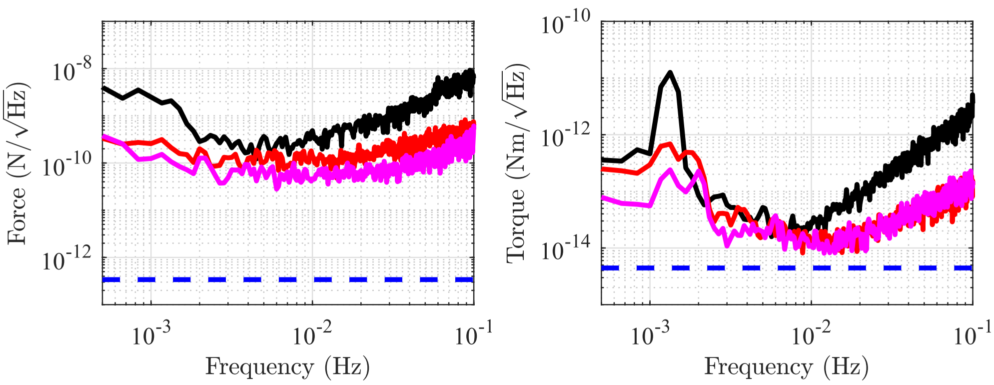

Figure 10. Residual force (left panel) and torque (right panel) ASD, measured with active compensation (magenta), no compensation (red) and before the upgrade (black). The dashed blue line is the expected thermal noise.

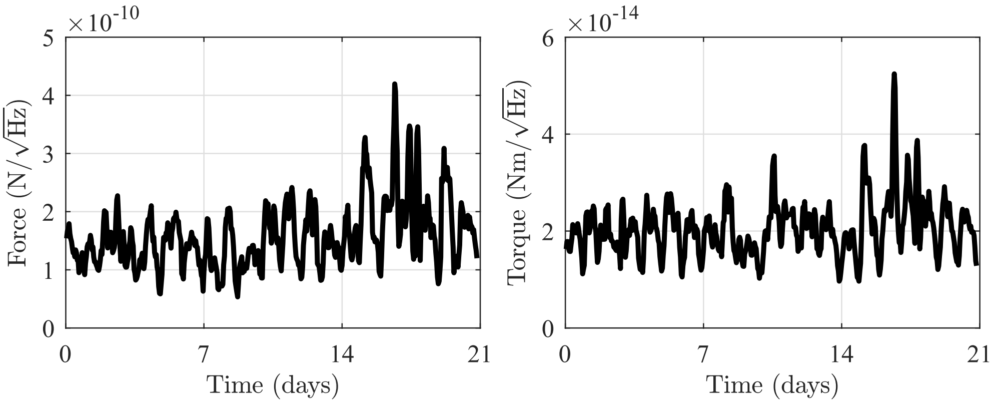

Figure 11. Value of the residual force (left panel) and torque (right panel), measured at $f = 10$ mHz during 3 week.

also reduces the effect of other disturbances (e.g. electronic noise and actuation noise) on the compensation signals.

In the best working conditions, with the compensation provided by the velocimeter, and the loops active to damp the low frequency torsion resonances, the pendulum was able to work for several weeks in high sensitivity mode. In figure 10 the ASD of the residual force and torque noises, observed in a period of 5 h, during a three weeks long run, are shown compared with the ones reported in figure 3. The expected thermal noise limit is also shown.

The lowest force noise ASD, in a small band around $f = 10$ mHz is about $6 \cdot 10^{-11}$ N $(\sqrt{\text{Hz}})^{-1}$, while the torque noise ASD, in the same band, is about 10^{-14} Nm $(\sqrt{\text{Hz}})^{-1}$.

It is worth noting that the improvement in force is due to better environmental condition and not to the compensation, that only acts at higher frequency. Nevertheless the compensation, providing an higher duty-cycle, increases the probability to operate the pendulum in high sensitivity condition during the periods of favorable environmental conditions.

Figure 11 shows the force and torque noise at $f = 10$ mHz during the three weeks of observation. In the left panel the force is reported, while in the right one there is the torque. Each value of force and torque was computed by using 5 h long ASDs.

6. Conclusion

This paper reports about the upgrades performed on the double torsion pendulum PETER aimed to enhance its sensitivity and duty-cycle. The upgrades, namely a rearrangement of the pendulum mechanics and the introduction of additional ORO allowed a reduction of a factor 5 in force noise and a factor 2 in torque noise (in the most sensitive frequency region around 10 mHz), with respect to the previous performances. Moreover, since the control of the suspension point is very effective in reducing the motion of the TM at the pendular resonance frequency, all the sensors can be used in high sensitivity mode, thus resulting in a large increase in the duty-cycle of the apparatus. In particular the system was able to operate in high sensitivity regime for longer than three weeks.

In these conditions, the pendulum residual noise, in terms of torque, is not far from the thermal noise limit: just a factor 3 in the frequency band from 4 to 20 mHz. This is not the case for the force noise that is still far from that limit. In this case the problem is due to the large translational motion of the pendulum that is largely due to the low frequency seismic noise.

This environmental noise, even after the upgrades, still shows a large coupling with the cross-bar rotation, while, thanks to the ORO, the sensing noise is well below the residual rotation noise. On the other hand no further direct coupling reduction are possible with the present set-up, nor compensation from the suspension point are possible since they would affect the measurement band.

The operation of the apparatus in a more quiet environment, with a lower seismic background noise, could certainly reduce also the force noise.

ORCID iDs

M Bassan https://orcid.org/0000-0001-6512-8003
R De Rosa https://orcid.org/0000-0002-4004-947X
L Di Fiore https://orcid.org/0000-0001-6296-1526
A Grado https://orcid.org/0000-0002-0501-8256
M Visco https://orcid.org/0000-0002-3515-6967

References

[1] Coulomb C A 1785 *Histoire de l'Acadmie R. Sci.* **88** 560–611
[2] Cavendish H 1798 *Phil. Trans. R. Soc.* **88** 469–526
[3] Rothleitner C and Schlamminger S 2017 *Rev. Sci. Instrum.* **88** 111101
[4] Li Q *et al* 2018 *Nature* **560** 582–8
[5] Murata J and Tanaka S 2015 *Class. Quantum Grav.* **32** 033001
[6] Sushkov A O, Kim W J, Dalvit D A R and Lamoreaux S K 2011 *Nat. Phys.* **7** 230–3
[7] Wagner T A, Schlamminger S, Gundlach J H and Adelberger E G 2012 *Class. Quantum Grav.* **29** 184002
[8] Carbone L, Cavalleri A, Dolesi R, Hoyle C D, Hueller M, Vitale S and Weber W J 2003 *Phys. Rev. Lett.* **91** 151101
[9] Cavalleri A *et al* 2009 *Class. Quantum Grav.* **26** 94017
[10] Stanga R *et al* 2009 *J. Phys.: Conf. Ser.* **154** 012032
[11] Dolesi R *et al* 2003 *Class. Quantum Grav.* **20** S99
[12] Antonucci F *et al* 2012 *Class. Quantum Grav.* **29** 124014
[13] Armano M *et al* 2016 *Phys. Rev. Lett.* **116** 231101
[14] Armano M *et al* 2017 *Phys. Rev.* D **96** 062004
[15] Armano M *et al* 2018 *Phys. Rev. Lett.* **120** 061101
[16] Antonucci F *et al* 2012 *Phys. Rev. Lett.* **108** 181101
[17] Bassan M *et al* 2016 *Phys. Rev. Lett.* **116** 051104
[18] Bassan M *et al* 2018 *Astropart. Phys.* **97** 19–26
[19] Brandt N *et al* 2008 LISA technology package experiment performance budget, Issue 2.4, ESA document reference: S2-ASD-RP-3036
[20] Bassan M *et al* 2019 Liquid actuated gravity experiments *Int. J. Mod. Phys.* D (accepted)
[21] Marconi L, Stanga R, Lorenzini M, Grimani C, Bassan M, Pucacco G, Di Fiore L, De Rosa R, Garufi F and Milano L 2010 *J. Phys.: Conf. Ser.* **228** 012037
[22] De Marchi F *et al* 2013 *Phys. Rev.* D **87** 122006
[23] Shimoda T, Aritomi N, Shoda A, Michimura Y and Ando M 2018 *Phys. Rev.* D **97** 104003
[24] De Rosa R, Di Fiore L, Garufi F, Grado A, La Rana A and Milano L 2011 *Astropart. Phys.* **34** 394–400
[25] Gualtieri L, Stutzmann E, Capdeville Y, Ardhuin F, Schimmel M, Mangeney A and Morelli A 2013 *Geophys. J. Int.* **193** 1732–45
[26] Weber W J, Bortoluzzi D, Cavalleri A, Carbone L, Da Lio M, Dolesi R, Fontana G, Hoyle C D, Hueller M and Vitale S 2003 *Proc. SPIE* **4856** 31–42
[27] Bassan M, De Marchi F, Marconi L, Pucacco G, Stanga R and Visco M 2013 *Phys. Lett.* A **377** 1555–62